

Electrochemical Synthesis of Efficient Catalyst Ni-Fe on Ni Foam for Electrochemical Water Splitting

NGUYEN THI MO^{1,*}, NGUYEN MINH CHAU¹, NGUYEN MINH BACH¹, PHAM QUANG DUC² and HOANG VAN HUNG^{1,*}

¹Faculty of Chemistry, Hanoi National University of Education, 136 Xuan Thuy, Cau Giay, Hanoi, Vietnam

²Archimedes Academy Secondary School, Trung Yen 10, Cau Giay, Hanoi, Vietnam

*Corresponding authors: Tel: +84 904530268, E-mail: ntmo@hnue.edu.vn; hungvh@hnue.edu.vn

Received: 25 September 2022;

Accepted: 4 July 2023;

Published online: 31 July 2023;

AJC-21325

Herein, the Ni-Fe electrocatalysts dispersed on nickel foam (NF) were successfully synthesized by the electrodeposition method. The electrode materials were characterized by XRD, EDX and SEM techniques. Electrochemical analysis was performed to determine the electrocatalytic properties for oxygen evolution reaction (OER) and hydrogen evolution reaction (HER) of the overall water splitting. The results indicate that the NiFe/NF electrode exhibits superior electrocatalytic activity as compared to the Ni/Fe and Fe/NF electrodes for both OER and HER with a significantly lower overpotential, 300 mV to reach 10 mA cm⁻² with OER and 364 mV to reach -20 mA cm⁻² with HER.

Keywords: Nickel, Iron, Electrochemical water splitting, Oxygen evolution reaction, Hydrogen evolution reaction.

INTRODUCTION

Electrocatalytic water splitting has been considered as a promising and feasible approach to the optimization of renewable energy conversion and the production of hydrogen, a clean sustainable energy carrier, could effectively solve the current energy crisis [1]. Electrocatalytic water splitting includes anodic oxygen evolution reaction (OER: $4\text{OH}^- \rightarrow \text{O}_2 + 2\text{H}_2\text{O} + 4\text{e}^-$) and cathodic hydrogen evolution reaction (HER: $2\text{H}_2\text{O} + 2\text{e}^- \rightarrow \text{H}_2 + 2\text{OH}^-$) [2]. Obviously, oxygen evolution reaction (OER) involves 4 electron transfer, while HER involves 2 electron transfer. Therefore, OER is a slow, rate-determining reaction. Hence, to enhance the efficiency of the overall water splitting process, efficient electrocatalysts are urgently demanded to accelerate the OER and minimize the overpotential [3,4].

To date, RuO₂ and IrO₂ based materials are accepted as the highly efficient OER electrocatalysts and Pt-based electrocatalysts show the highest activity for HER [4-8]. However, high price, poor stability and low storage of the noble and precious metal electrocatalysts have limited their large-scale application. Over the last few decades, great efforts have been devoted to exploring highly active earth-abundant and cost effective transition metal based catalysts such as Mo, W, Co, Ni, Fe, *etc.* for OER or HER [8-11].

Among transition metal based electrocatalysts, Ni-Fe-based materials are of great interest owing to their abundance in the earth's crust, low cost, low toxicity and high catalytic activity for various redox processes [8,12-16]. Recent studies have shown that Ni-Fe-based electrocatalysts exhibit high OH⁻ adsorption capacity, relatively low overpotential values, as well as high corrosion resistance in alkaline media [13,17,18]. The incorporation of Fe and Ni could effectively enhance the HER and OER performance [19-21]. Suryanto *et al.* [8] explained that the unusually high electrocatalytic activity of the Ni-Fe electro-catalyst was attributed to the interfacial electronic coupling effect due to the asymmetrical distribution of Ni and Fe₂O₃ in the electrocatalyst. Li *et al.* [12] investigated the impact of Fe(OH)₃ colloids on the OER activity of NiFeOH and figured out that Fe(OH)₃ nanoparticles can promote the accumulation of Fe on the surface of anode. The charge can be transferred from Ni²⁺ to Fe³⁺ more quickly; hence, the adsorption of active oxygen is accelerated and electron-transfer kinetics of OER can be enhanced. Therefore, the catalytic activity of NiFeOH toward OER can be built up about 40 times owing to Fe(OH)₃ nanoparticles adsorbed onto NiFeOH [12]. Additionally, combining electrocatalysts with a highly conductive substrate such as nickel foam, carbon paper and graphene can effectively reduce the internal impedance and facilitate charge transport, there-

fore, significantly enhances their catalytic activity and stability [2,22,23]. Due to its high electronic conductivity, good electrical conductivity and 3D open-pore structure [2], Ni foam is regarded as a potential candidate for optimizing the nanostructure of electro-catalysts.

Herein, NiFe electrocatalysts were prepared on Ni foam (NiFe/NF) by the electrodeposition method. The NiFe/NF functions with lower overpotentials than the Ni/NF and Fe/NF for both OER and HER. In 1 M KOH electrolyte, the overpotentials of NiFe/NF were 300 mV to reach 10 mA cm⁻² in the anode and 364 mV to reach -20 mA cm⁻² in the cathode.

EXPERIMENTAL

The chemicals *viz.* Ni(NO₃)₂·6H₂O, FeCl₃·6H₂O and KOH used in this study were purchased from China. All chemicals were of analytical grade and used as received without further purification. Nickel foam (NF) with a thickness of 1.0 mm was purchased from China and cut into pieces of 1 cm × 3 cm. The nickel foam was ultrasonicated in 3 M HCl for 30 min to withdraw the surface oxides and ultrasonicated in acetone for 30 min to take off the organic matter, washed 3 times with water and thrice with ethanol then dried at 50 °C for 2 h.

The Ni-Fe electrocatalyst on the Ni foam was synthesized *via* the electrodeposition method using a three-electrode system consisting of Ni foam working electrode, Pt counter electrode and Ag/AgCl (saturated KCl) reference electrode. The electrolyte consisted of 3 mM Ni(NO₃)₂ and 3 mM Fe(NO₃)₃. A nickel iron thin film was deposited on the NF substrates by using chronoamperometry method at -1.0 V (*vs.* Ag/AgCl) for 300 s at room temperature. After deposition, the working electrode was carefully taken out, rinsed several times using distilled water, followed by ethanol, then dried at 40 °C for 4 h. Finally, the fabricated electrode was calcined at 500 °C in an Argon atmosphere for 5 h and was labelled as NiFe/NF.

For comparison, Ni/NF and Fe/NF electrodes were also fabricated using the same procedure, replacing the electrolyte solution with solutions containing only 3 mM Ni(NO₃)₂ or 3 mM Fe(NO₃)₃, respectively.

Characterization: X-ray diffraction method (XRD) was performed with a Bruker-D5005 diffractometer using CuK α irradiation with $\lambda = 1.5406 \text{ \AA}$ at 40 kV and 100 mA to determine the structure of the materials.

Scanning electron microscopy (SEM) was acquired on a SEM-JEOL JSM.5410LV scanning electron microscope at an accelerating voltage of 5 kV to determine the morphology of the samples. The elemental composition of the samples was proved by utilizing energy-dispersive X-ray spectroscopy (EDX) in a JEOL SEM-6510LV 5410LV scanning electron microscope using an X-act Oxford Instruments X-ray analyzer.

Electrochemical measurements: Electrochemical measurements were performed using an Autolab 302N electrochemical workstation in a three-electrode system with 1 M KOH electrolyte at room temperature. The synthesized material was used as the working electrode immersed in the KOH solution with an area of 1 cm × 1 cm. A platinum rod and Ag/AgCl (saturated KCl) were used as counter and reference electrodes, respectively. The electrochemical performance of all prepared

electrodes was evaluated using linear sweep voltammetry (LSV) for HER and the OER with the scan rate of 10 mV s⁻¹. EIS of the samples was performed with frequencies ranging from 10 KHz to 100 mHz. All potentials were converted into the RHE scale using eqn. 1:

$$E_{\text{RHE}} = E_{\text{Ag/AgCl}} + E_{\text{Ag/AgCl vs. NHE}} + 0.059 \text{ pH} \quad (1)$$

where $E_{\text{AgCl vs. NHE}} = 0.1976 \text{ V}$ at 20 °C.

The Tafel slope (b) was calculated through determined overpotential (η) and measured current density j using the equation:

$$\eta = b \log j + a \quad (2)$$

where, a is a constant.

RESULTS AND DISCUSSION

XRD studies: An X-ray diffraction method was employed to determine the structure of the samples and the results are shown in Fig. 1. Obviously, in the XRD patterns of all samples, three diffraction peaks are observed at the values of $2\theta = 44.7^\circ$, 52.1° and 76.5° corresponding to the facets: (111), (200) and (220), indicative of the structure of nickel in the nickel foam (NF) (JCPDS card no. 04-0850). The X-ray diffraction pattern of NiFe/NF sample features no specific diffraction peaks of other crystalline structures. Therefore, Ni and Fe are probably dispersed on the surface of NF with low crystallinity or in the amorphous form.

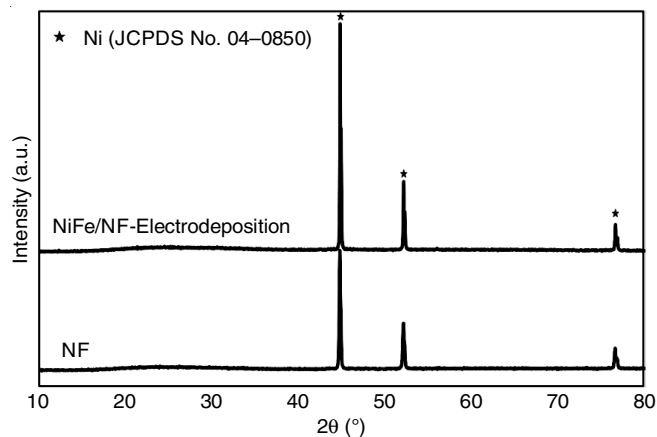


Fig. 1. XRD patterns of nickel foam (NF) and NiFe/NF

EDX studies: The elemental composition of the electrocatalyst samples was determined by the EDX method. The results are shown in Fig. 2 and Table-1. It is obvious that a relatively great amount of O and C is present on the surface of the samples. It can also be observed that in the NF sample, Fe content is very low, accounting for only 0.6%. After nickel and iron were deposited on the NF surface, the Fe content in the material increased significantly to 4.5%. The Ni-Fe:O molar ratio is significantly less than 1, indicating that there are probably metallic nickel and metallic iron formed on the surface of NF.

SEM studies: SEM images of synthesized electrocatalysts are displayed in Fig. 3. The surface of cleaned NF is quite rough, probably leading to the formation of surface defects, which facilitates the adsorption of other components to the surface

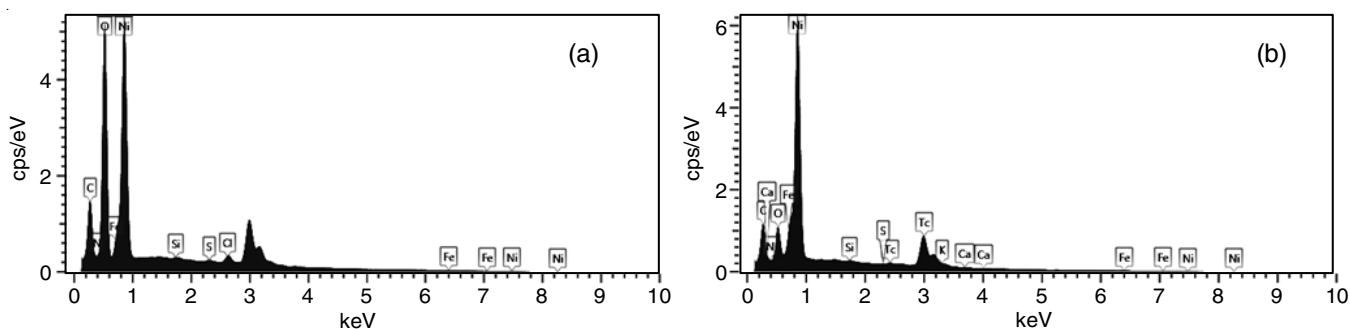


Fig. 2. EDX spectra of nickel foam (NF) (a) and NiFe/NF (b)

TABLE-1
ELEMENTAL COMPOSITION OF THE SAMPLES

	Atomic percentage (%) of elements						
	Ni	Fe	O	S	N	C	Others
NF	24.5	0.6	46.4	0.1	5.4	22.0	1.0
NiFe/NF	48.6	4.5	13.4	0.1	1.1	31.4	0.9

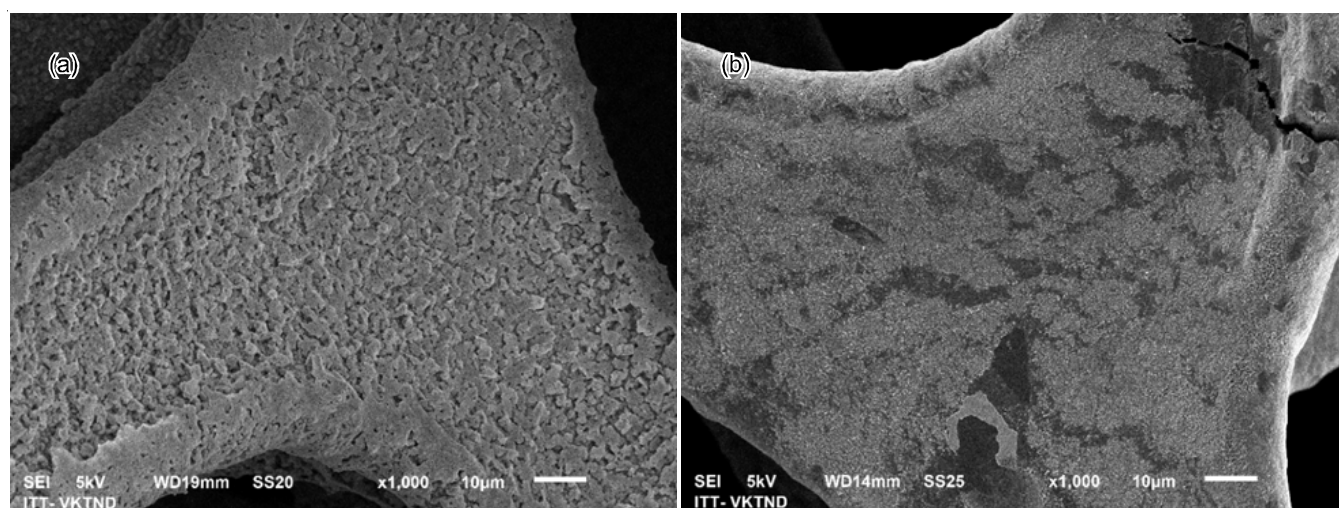


Fig. 3. SEM images of nickel foam (NF) (a) and NiFe/NF (b)

of NF. A thin film coating appears on the surface of NF after nickel and iron are electrochemically deposited on the NF surface. The coating layer is formed on the NF surface as tiny nanoparticles however, the coating layer is not uniform.

Electrochemical measurements: To evaluate the electrocatalytic performance of synthesized materials for OER, HER and the charge transfer ability of the materials, LSV and EIS methods were carried out in 1.0 M KOH solution with the use of a traditional three-electrode system and the results are shown in Fig. 4. From the LSV curve for OER in Fig. 4a, it is worth to mention that the synthesized electrocatalysts exhibit high OER performance with low over potentials to drive the current density of 10 mA cm^{-2} , which are 370 mV, 354 mV and 300 mV for Ni/NF, Fe/NF and NiFe/NF, respectively while with the same current density of 10 mA cm^{-2} , the overpotential for NF is 390 mV. Moreover, it is obvious that the OER activity of electrocatalysts is promoted when depositing nickel and iron on the surface of NF, since the LSV curve shifts to the lower potential direction and the overpotential values of Ni-Fe deposited samples are lower than those of NF at all measured current densities.

Obviously, the combination of Ni and Fe significantly increases the electrocatalytic activity of the materials.

To provide more insight into the reaction kinetics of OER of the synthesized materials, the Tafel curves were obtained using Tafel equation $\eta = \text{blog}(j) + a$ and the results are depicted in Fig. 4b. Tafel slopes for NF, Ni/NF, Fe/NF and NiFe/NF samples were determined to be 195 mV dec^{-1} , 184 mV dec^{-1} , 149 mV dec^{-1} and 81 mV dec^{-1} , respectively. Hence, Ni/NF and Fe/NF exhibit enhanced kinetics for OER with a lower Tafel slope as compared to NF. The result also confirms the superior OER kinetics of the combined NiFe/NF sample with a much lower Tafel slope, 81 mV dec^{-1} .

Similarly, as in Fig. 4c, it should be pointed out that Ni/NF and Fe/NF exhibit a lower overpotential than NF and NiFe/NF shows the lowest overpotential at all ranges of determined current densities. The LSV curve of the samples shifts to a less negative potential direction as compared to the LSV curve of NF. This indicates that the HER occurs more easily on the electrodes containing the Ni and Fe catalysts and occurs most easily on the NiFe/NF electrode. The overpotential for the HER to reach

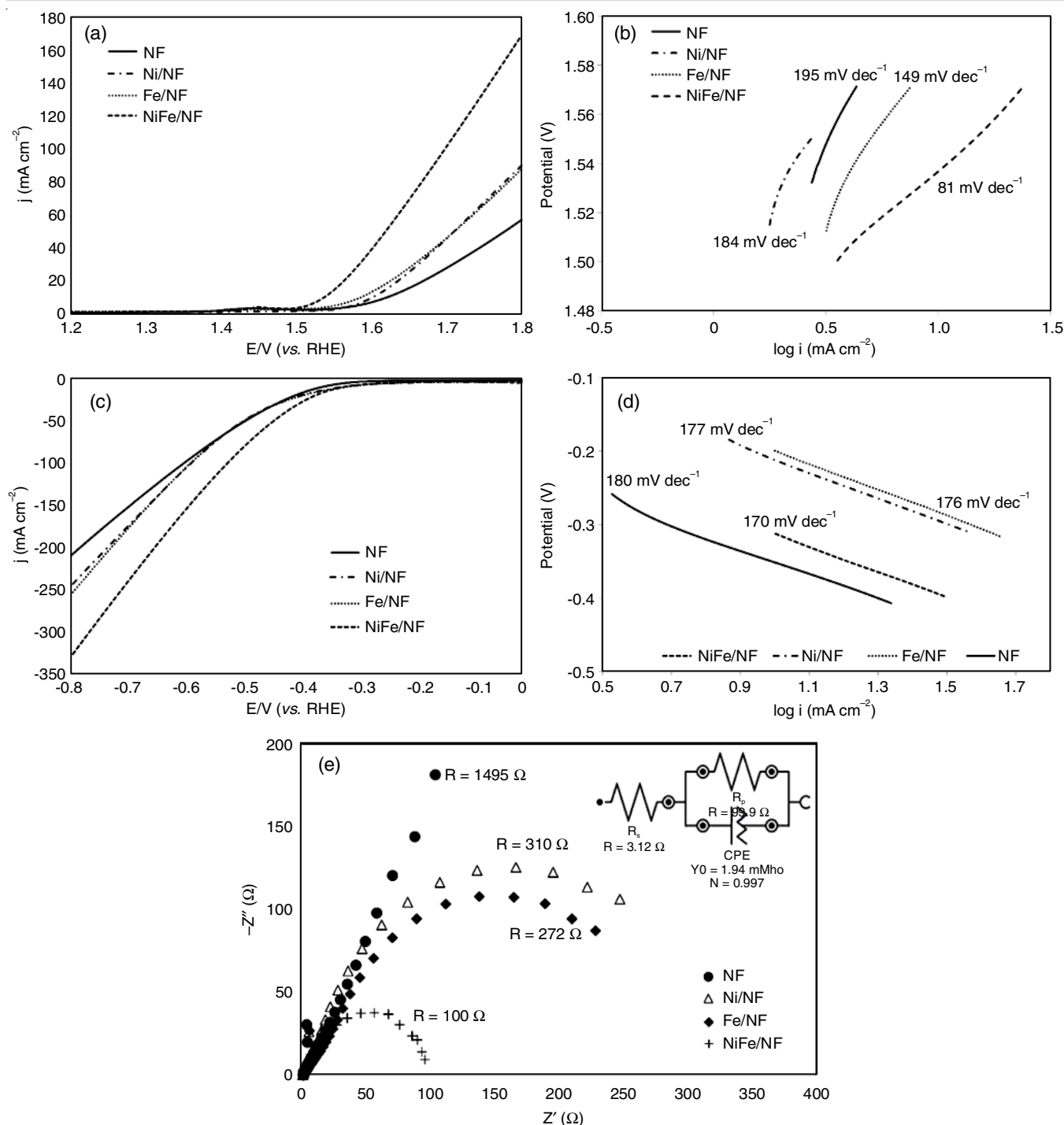


Fig. 4. Electrochemical properties of nickel foam (NF), Fe/NF, Ni/NF and NiFe/NF: (a) LSV curve for OER; (b) Tafel plot for OER; (c) LSV curve for HER; (d) Tafel plot for HER; (e) Nyquist plot

the current density of -20 mA cm⁻² for the NF, Ni/NF, Fe/NF and NiFe/NF electrodes is: 400 mV, 389 mV, 386 mV and 364 mV, respectively. Their corresponding Tafel slopes were 180 mV dec⁻¹, 177 mV dec⁻¹, 176 mV dec⁻¹ and 170 mV dec⁻¹, respectively (Fig. 4d), implying enhanced kinetics for HER of synthesized samples. Furthermore, EIS was performed over the frequency range from 100 mHz to 100 kHz under OER to study the charge transfer and evaluate the interfacial reactions of the synthesized materials. The intercept on Z' axis and the

semicircle (Fig. 4e) in the Nyquist plot can be assigned to the electrolyte solution resistance (R_s) and charge transfer resistance (R_{ct}), respectively. The value of the electrolyte resistance, R_s in the equivalent circuit, is similar for all electrodes (3.12 Ω).

The charge-transfer resistance value (R_{ct} in the equivalent circuit) of the electrodes decreases in the order: NF (1495 Ω) > Ni/NF (310 Ω) > Fe/NF (272 Ω) > NiFe/NF (100 Ω). This order is also consistent with the trend in overpotential and Tafel slope. FeNi/NF exhibits the smallest semicircle diameter value,

indicating the fastest shuttling of charge transfers and facilitating the migration of electron back and forth in the interface between the electrolyte solution and the electrode. The smaller R_{ct} of NiFe/NF value also implies a faster Faradaic process and better OER kinetics. As shown in the inset figure attached to Fig. 4e, the equivalent circuit includes a resistor parallel with a capacitor, indicating good contact between the catalyst and the conductive substrate.

Conclusion

In summary, nickel and iron were successfully loaded on Ni foam by employing the electrodeposition method. They are well dispersed on the surface of nickel foam (NF) with low crystallinity. The electrodes exhibit high electrocatalytic activity for both oxygen evolution reaction (OER) and hydrogen evolution reaction (HER). The prepared NiFe/NF material reveals lower overpotential of OER and HER as well as the charge transfer resistance on the electrode surface than those of both Fe/NF and Ni/NF materials. It exhibits lower OER overpotential, 300 mV, to afford a current density of 10 mA cm⁻² and lower HER overpotential of 364 mV to gain a current density of -20 mA cm⁻² with a charge-transfer resistance of 100 Ω. Therefore, the Ni-Fe-based electrocatalyst material has great potential for application as an electrode material for overall electrochemical water splitting.

ACKNOWLEDGEMENTS

This research is funded by the Ministry of Education and Training under grant number B2022-SPH-15.

CONFLICT OF INTEREST

The authors declare that there is no conflict of interests regarding the publication of this article.

REFERENCES

- S. Lee, H. Kim, W. Lee and J. Kim, *Nano-Micro Lett.*, **6**, 1 (2018); <https://doi.org/10.1186/s40486-018-0063-4>
- S. Ren, X. Duan, F. Ge, M. Zhang and H. Zheng, *J. Power Sources*, **480**, 228866 (2020); <https://doi.org/10.1016/j.jpowsour.2020.228866>
- C. Feng, M.B. Faheem, J. Fu, Y. Xiao, C. Li and Y. Li, *ACS Catal.*, **10**, 4019 (2020); <https://doi.org/10.1021/acscatal.9b05445>
- S.H. Park, S.H. Kang and D.H. Youn, *Materials*, **14**, 4768 (2021); <https://doi.org/10.3390/ma14164768>
- X. Zou, Y. Wu, Y. Liu, D. Liu, W. Li, L. Gu, H. Liu, P. Wang, L. Sun and Y. Zhang, *Chem*, **4**, 1139 (2018); <https://doi.org/10.1016/j.chempr.2018.02.023>
- K. Liang, L. Guo, K. Marcus, S.F. Zhang, Z. Yang, D.E. Perea, L. Zhou, Y. Du and Y. Yang, *ACS Catal.*, **7**, 8406 (2017); <https://doi.org/10.1021/acscatal.7b02991>
- R. Li, Y. Li, P. Yang, D. Wang, H. Xu, B. Wang, F. Meng, J. Zhang and M. An, *J. Energy Chem.*, **57**, 547 (2021); <https://doi.org/10.1016/j.jechem.2020.08.040>
- B.H.R. Suryanto, Y. Wang, R.K. Hocking, W. Adamson and C. Zhao, *Nat. Commun.*, **10**, 5599 (2019); <https://doi.org/10.1038/s41467-019-13415-8>
- F. Yu, H. Zhou, Y. Huang, J. Sun, F. Qin, J. Bao, W.A. Goddard III, S. Chen and Z. Ren, *Nat. Commun.*, **9**, 2551 (2018); <https://doi.org/10.1038/s41467-018-04746-z>
- C. Xuan, J. Wang, W. Xia, Z. Peng, Z. Wu, W. Lei, K. Xia, H.L. Xin and D. Wang, *ACS Appl. Mater. Interfaces*, **9**, 26134 (2017); <https://doi.org/10.1021/acsami.7b08560>
- J. Li, S. Wang, J. Chang and L. Feng, *Adv. Powder Mater.*, **1**, 100030 (2022); <https://doi.org/10.1016/j.apmate.2022.01.003>
- Q. Li, T. He, X. Jiang, Y. Lei, Q. Liu, C. Liu, Z. Sun, S. Chen and Y. Zhang, *J. Colloid Interface Sci.*, **606**, 518 (2022); <https://doi.org/10.1016/j.jcis.2021.08.037>
- S.-H. Cai, X.-N. Chen, M.-J. Huang, J.-Y. Han, Y.-W. Zhou and J.-S. Li, *J. Mater. Chem. A Mater. Energy Sustain.*, **10**, 772 (2022); <https://doi.org/10.1039/D1TA08385F>
- J. Cirone, J.S. Dondapati and A. Chen, *Electrochim. Acta*, **392**, 139016 (2021); <https://doi.org/10.1016/j.electacta.2021.139016>
- Q. Wu, S. Wang, J. Guo, X. Feng, H. Li, S. Lv, Y. Zhou and Z. Chen, *Nano Res.*, **15**, 1901 (2022); <https://doi.org/10.1007/s12274-021-3800-6>
- M. Zhao, J. Du, H. Lei, L. Pei, Z. Gong, X. Wang and H. Bao, *Nanoscale*, **14**, 3191 (2022); <https://doi.org/10.1039/D1NR08035K>
- K.H. Kim, J.Y. Zheng, W. Shin and Y.S. Kang, *RSC Adv.*, **2**, 4759 (2012); <https://doi.org/10.1039/c2ra20241g>
- P. Ganesan, A. Sivanantham and S. Shanmugam, *J. Mater. Chem. A Mater. Energy Sustain.*, **4**, 16394 (2016); <https://doi.org/10.1039/C6TA04499A>
- Q. Yan, T. Wei, J. Wu, X. Yang, M. Zhu, K. Cheng, K. Ye, K. Zhu, J. Yan, D. Cao, G. Wang and Y. Pan, *ACS Sustain. Chem. Eng.*, **6**, 9640 (2018); <https://doi.org/10.1021/acssuschemeng.7b04743>
- G. Zhang, Y.S. Feng, W.T. Lu, D. He, C.Y. Wang, Y.K. Li, X.Y. Wang and F.F. Cao, *ACS Catal.*, **8**, 5431 (2018); <https://doi.org/10.1021/acscatal.8b00413>
- Q.-Q. Chen, C.-C. Hou, C.-J. Wang, X. Yang, R. Shi and Y. Chen, *Chem. Commun.*, **54**, 6400 (2018); <https://doi.org/10.1039/C8CC02872A>
- C.Z. Yuan, Z.T. Sun, Y.F. Jiang, Z.K. Yang, N. Jiang, Z.W. Zhao, U.Y. Qazi, W.H. Zhang and A.W. Xu, *Small*, **13**, 1604161 (2017); <https://doi.org/10.1002/smll.201604161>
- X. Bu, R. Wei, Z. Cai, Q. Quan, H. Zhang, W. Wang, F. Li, S.P. Yip, Y. Meng, K.S. Chan, X. Wang and J.C. Ho, *Appl. Surf. Sci.*, **538**, 147977 (2021); <https://doi.org/10.1016/j.apsusc.2020.147977>